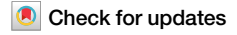
Published in partnership with King Fahd University of Petroleum & Minerals



https://doi.org/10.1038/s41545-024-00301-0

Highly permeable and shelf-stable aquaporin biomimetic membrane based on an anodic aluminum oxide substrate



Ahmed Fuwad¹², Hyunil Ryu³, Eui Don Han⁴, Jun-Hee Lee⁵, Noah Malmstadt⁶, Young-Rok Kim®⁵, Young Ho Seo⁴, Sun Min Kim®¹,₃७ & Tae-Joon Jeon®³,⋼ ⊠

Aquaporin (AQP) biomimetic membranes are a coming-of-age technology for water purification. Although several studies have reported aquaporin biomimetic membrane fabrication to date, these membranes show low water flux mainly due to the low porosity and inherently dense structure of the polymeric substrate materials. Herein, we report a ceramic-based aquaporin biomimetic membrane based on anodic aluminum oxide (AAO) as a substrate, which has a uniform porous structure with a high aspect ratio and pore density compared to conventional polymer substrates and exhibits a high water flux of 27.6 ± 3.6 LMH (L m⁻² h⁻¹) and superior membrane selectivity of 0.11 g L⁻¹. Briefly, the AAO substrate was functionalized with amino-silane followed by polydopamine coating, then the AQP vesicles were immobilized on the functionalized AAO substrate surface using an electrokinetic method, and the water rejection performance of the membrane was analyzed in a forward osmosis system. Furthermore, a simple cryodesiccation method is introduced to improve the storage stability and easy transportation of aquaporin membranes, which does not require special environmental conditions to transport or store them.

Recent developments in nanobiotechnology have shown the potential to impact a diverse range of conventional industrial technologies, including water desalination, by enabling the incorporation of active biomolecules into novel membrane designs. In fact, a tremendous amount of research using novel nanobiotechnology has been carried out for the development of better water treatment techniques. Since the discovery of water-selective proteins, aquaporins (AQPs) have been identified as an ideal molecular tool for fabricating a water desalination membrane with water-selective channels¹. AQPs are specialized proteins dedicated to facilitating water transport across cellular membranes, thereby maintaining water homeostasis. An AQP forms a cylindrical channel pore within the hydrophobic region of the membrane with a diameter of 3 Å, which allows only a single file of water molecules for transportation. The arginine residue at the center of the protein interacts with water molecules by forming a hydrogen bond, effectively excluding other molecules or ions from passing through the

channel^{2,3}. Recent studies have explored the use of AQP proteins in biomimetic membranes as a promising approach to developing novel materials for water treatment applications^{4,5}.

To improve the feasibility of water-selective biomimetic membranes, a number of different approaches to fabricate AQP biomimetic membranes have been reported, including liposome adsorption, chemical crosslinking, interfacial polymerization, magnetic-aided adsorption and electrokinetic interaction of linear li

¹Department of Mechanical Engineering, Inha University, Incheon 22212, Korea. ²Department of Biomedical Engineering and Sciences, School of Mechanical and Manufacturing Engineering (SMME), National University of Sciences and Technology (NUST), Islamabad 44000, Pakistan. ³Department of Biological Sciences and Bioengineering, Inha University, Incheon 22212, Korea. ⁴Department of Mechatronics Engineering, Kangwon National University, Chuncheon 24341, Korea. ⁵Institute of Life Sciences and Resources & Department of Food Science and Biotechnology, Kyung Hee University, Yongin 17104, Korea. ⁶Mork Family Department of Chemical Engineering & Materials Science, University of Southern California, Los Angeles, CA 90089, USA. ⁷Biohybrid Systems Research Center (BSRC), Inha University, Incheon 22212, Korea. ⁸Department of Biological Engineering, Inha University, Incheon 22212, Korea. ⁸Department of Biological Engineering, Inha University, Incheon 22212, Korea. ⁸Department of Biological Engineering, Inha University, Incheon 22212, Korea. ⁸Department of Biological Engineering, Inha University, Incheon 22212, Korea. ⁸Department of Biological Engineering, Inha University, Incheon 22212, Korea. ⁸Department of Biological Engineering, Inha University, Incheon 22212, Korea. ⁸Department of Biological Engineering, Inha University, Incheon 22212, Korea. ⁸Department of Biological Engineering, Inha University, Incheon 22212, Korea. ⁸Department of Biological Engineering, Inha University, Incheon 22212, Korea. ⁸Department of Biological Engineering, Inha University, Incheon 22212, Korea. ⁸Department of Biological Engineering, Inha University, Incheon 22212, Korea. ⁸Department of Biological Engineering, Inha University, Incheon 22212, Korea. ⁸Department of Biological Engineering, Inha University, Incheon 22212, Korea. ⁸Department of Biological Engineering, Inha University, Incheon 22212, Korea. ⁸Department of Biological Engineering, Inha University, Incheon 22212, Korea. ⁸Department of Biologic

contrast, the TFN design, favored for its ease of scalable fabrication through polymerization of an AQP-containing selective layer onto a porous substrate, is more widely adopted. However, optimizing TFN polymer matrices to maintain AQP function remains a significant area of focus¹². Therefore, advancing AQP biomimetics requires a careful balance between the opportunities and limitations of each design strategy¹³. Previous studies utilized polymeric substrates that are characterized by low surface porosity and non-uniformity, primarily due to their structural and material characteristics. This results in increased pore localization, leading to a longer effective diffusion path for water molecules through the selective layer before desorbing into the pores of the support layer. Consequently, this limitation significantly restricts the water permeability through the active AQP biomimetic membranes, affecting the potential applications of the system¹⁴. Additionally, to mitigate the low permeability of conventional polymeric membranes, a support layer with a highly porous microstructure consisting of a repeating finger-like structure was devised instead of the conventional sponge-like configurations typically observed in polymeric membranes tailored for high-pressure applications¹⁴⁻¹⁷. Similarly, in another study, an ion-track etching method produces linear channels similar to uniform pores, but ion-track-etched membranes display a very low porosity that reduces water transport^{18,19}. Moreover, AQP biomimetic membranes require specific environmental conditions, including tightly controlled ranges of humidity and temperature, for their transportation and storage^{20,21}. These requirements preclude their practical use in commercial applications.

To address the above problems, we developed a ceramic anodic aluminum oxide (AAO)-based AQP biomimetic membrane. The AAO substrates can achieve a uniform porous structure with a high aspect ratio and pore density compared to conventional polymer substrates^{22,23}. The unique honeycomb-like surface and cylindrical pore structure of AAO promotes stable immobilization of AQP vesicles on the surface, with high water permeability performance. The previous study on the fabrication of AAOsubstrate-based biomimetic membranes shows defects in the coating, resulting in low salt rejection performance²⁴. This was mainly due to the high surface roughness, incomplete functionalization, and most importantly, uncontrolled coating methodology of AQP liposomes on the substrate, which leads to uneven coating of AQP coating on the substrate. Herein, we addressed these issues by synthesizing the AAO substrate via a one-step alumina anodization process (Fig. 1); which reduces the surface roughness of the substrate compared to the conventionally prepared two-step anodization process, then functionalizing the substrate with polydopamine, which further smoothens the surface and acts as a cushioning layer for AQP liposomes during coating. Finally, the functionalized AAO substrate was coated with electrokinetically driven AQP liposomes. The smooth surface, uniform pore distribution, and smaller pore size of the AAO substrate compared to AQP liposomes enabled defect-free, high-density immobilization of vesicles. As a result, the membrane showed superior water desalination performance with a water flux of 27.6 ± 3.6 LMH and a superior membrane selectivity of 0.11 g L⁻¹ in the active layer feed side mode (AL-FS). Furthermore, to increase the storability and transportability of the AQP membrane, the AQP vesicle-coated membrane was subjected to a cryodesiccation process^{25–27}. The membrane was then rehydrated at 4 °C to recover its structure and functions. The performance of the rehydrated membrane was analyzed through forward osmosis (FO) water purification, and it showed almost the same performance as before cryodesiccation. In short, our research brings AQP-based water purification membranes one step closer to practical application by overcoming the two most critical problems: low permeability of the supporting material and poor storability at ambient conditions due to the characteristics of biomimetic membranes.

Results and discussion Characterization of AAO substrates

The surface morphology of a substrate plays an important role in the fabrication of AQP biomimetic membranes; therefore, we analyzed the surface morphology of the AAO substrate through FESEM and AFM. Generally, an AAO substrate is fabricated through a 2-step anodic aluminum oxidation process to achieve a uniform honeycomb array of nanoporous structures²⁸. This 2-step anodic oxidation process increases the surface roughness of the AAO substrate mainly due to the self-alignment of the porous layer during the first step of anodization as a base for nanopores formed in the second anodization process, which results in the formation of a nanodimple pattern, increasing the surface roughness. Figure 2a, b shows FESEM images of inclined AAO substrate after one (Fig. 2b) and two (Fig. 2a) steps of anodic oxidation. The presence of nanodimples can easily be seen in Fig. 2a, while they are absent in Fig. 2b, which consequently reduces the surface roughness of the AAO substrate. The surface roughness (Rq) of the 2-step sample is 35.9 nm, whereas that of the 1-step sample is 19.6 nm, as shown in Fig. 2c, d. Channel-type pore formation using the 1-step anodic aluminum oxidation was verified by taking a cross-sectional image of AAO substrates. The pore size was measured using a previously published computational image processing method²⁹ and 100 FESEM images of each of the AAO samples. Furthermore, the effectiveness of 1-step anodic aluminum oxidation in producing channel-like through pores was verified by analyzing the crosssectional FESEM images of AAO substrates. Figure 2e-h shows the cylindrical pore structure of different AAO substrates with diameters ranging from 50 to 125 nm. This demonstrates that through 1-step anodic

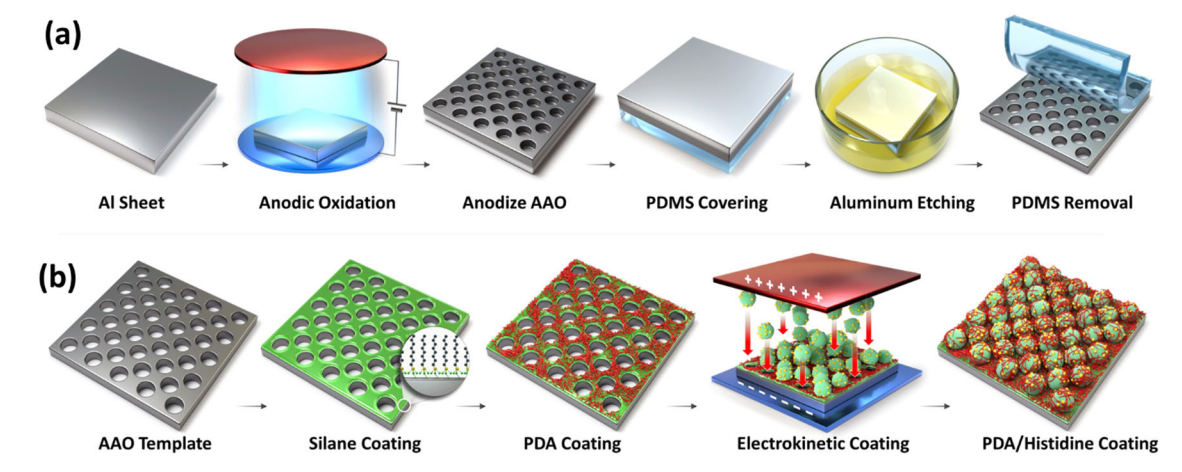
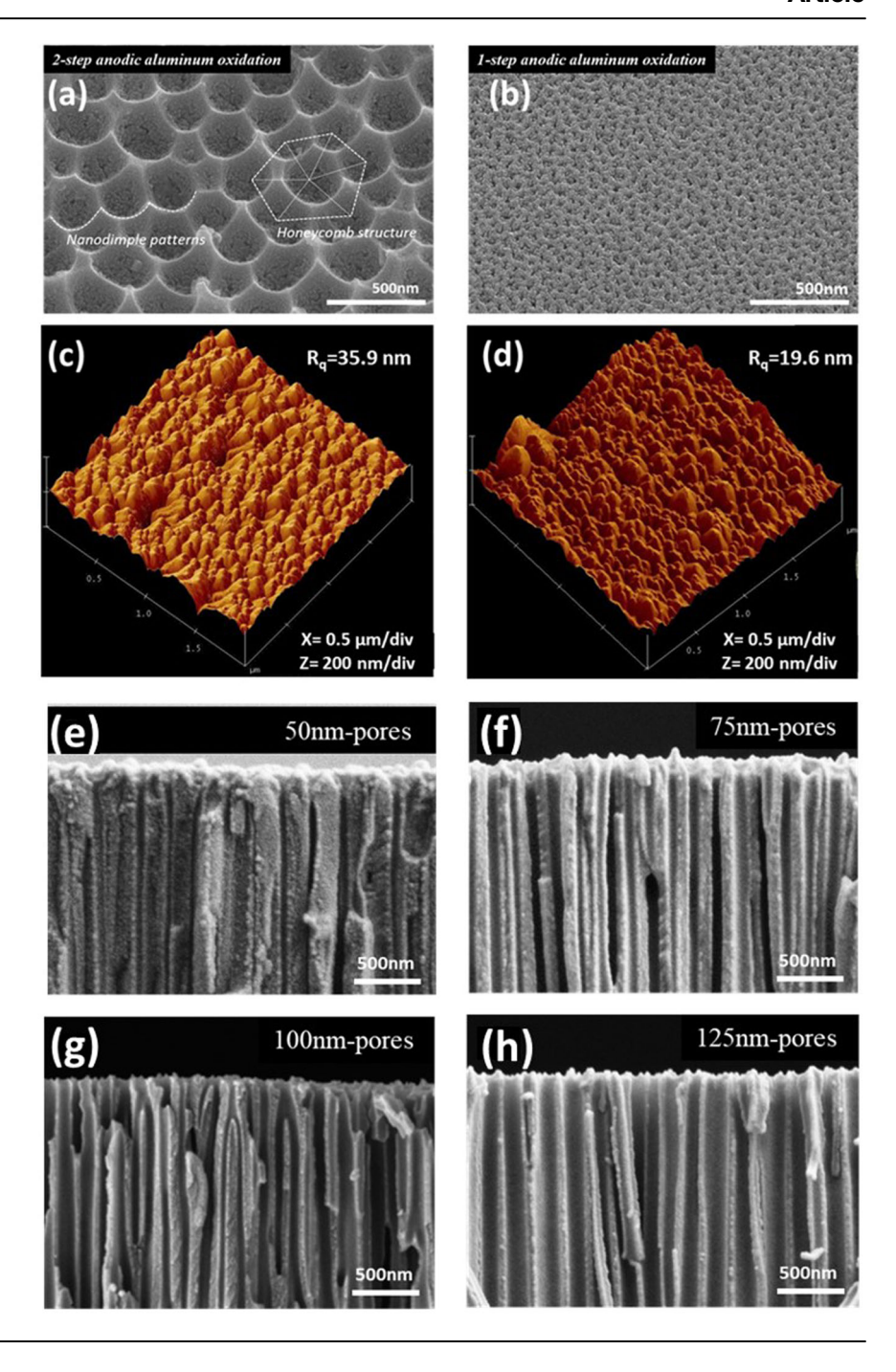


Fig. 1 | **Schematic presentation of the substrate. a** AAO substrate fabrication process and **b** surface functionalization scheme of the AAO membrane with silane followed by sequential PDA coating and AQP liposome immobilization. The functionalization process increases the membrane stability and performance by

enabling uniform coating of AQP liposomes on the surface. The silane and PDA coating on the substrate surface decreases surface roughness and provides cushioning support to the AQP liposomes. Under the applied electric field, the charged liposomes can easily move to the smooth surface for uniform immobilization.

Fig. 2 | Surface morphological analysis of AAO membranes. a Inclined image of an AAO substrate fabricated using the general 2-step anodic aluminum oxidation process. The formation of nanodimples is marked by dotted lines. b AAO substrate fabricated using the 1-step anodic aluminum oxidation process. c AFM analysis of 2-step anodic aluminum oxidation substrate, showing an Rq of 35.6 nm. d AFM analysis of the 1-step anodic aluminum oxidation substrate, showing an Rq of 19.6 nm. e-h Cross-sectional FESEM images of different AAO substrates fabricated through a 1-step anodic aluminum oxidation process. e 50 nm pore diameter with etching time ~75 min. f 75 nm pore diameter with etching time ~115 min. g 100 nm diameter etching time ~150 min and h 125 nm pore diameter with etching time ~190 min. The scale bar in \mathbf{a} , \mathbf{b} and \mathbf{e} - \mathbf{h} are 500 nm.



aluminum oxidation, a uniform cylindrical channel-like porous substrate with a wide range of controlled pore sizes can easily be synthesized with minimum surface roughness.

Characterization of AqpZ protein and AqpZ liposomes

SDS–PAGE analysis was performed on each fraction from the purification process. It was confirmed that GFP-AqpZ was expressed and purified by the major band (red box, size $\sim\!\!70\,\mathrm{kDa})$ of the elution fraction (Fig. 3a). In addition, the green fluorescence of the purified protein was confirmed by microscopy (Fig. 3b), indicating the successful fusion expression and purification of GFP-AqpZ. The presence of AqpZ in liposomes affects their structural characteristics and alters their properties, including size and surface charge. The size analysis of liposomes before and after AqpZ incorporation was analyzed by DLS intensity analysis in Fig. 3c. The liposomes show an average size $(Z_{\rm avg})$ of $164\pm44\,\mathrm{nm}$ with a polydispersity

(PDI) of 0.236 ± 0.151 , while the AQP liposomes show a decrease in size to 134 ± 21 nm with a PDI of 0.015 ± 0.002 , the low PDI shows a uniform size distribution of AQP liposomes in solution, which is a highly required attribute for water permeability performance as well as uniform coating on the substrate surface. The decrease in liposome size is due to the bending and compression of the lipid membrane near the extracellular region of the AQP protein Similarly, the AQP surface contains a strong negative charge, which changes the liposome charge from slightly positive $(1.41\pm0.1.2 \text{ mV})$ to strongly negative $(-17.44\pm2.3 \text{ mV})$ in Fig. 3d. These observations validate the high incorporation efficiency of AQPs into liposomes with uniform size distribution and surface charge, a prerequisite for the fabrication of high-performance AQP biomimetic membranes. Furthermore, the activity of AQP liposomes was analyzed using a stopped-flow light scattering apparatus. The analysis was performed on liposomes with and without AQPs. The sample solution was mixed in a fixed ratio with a

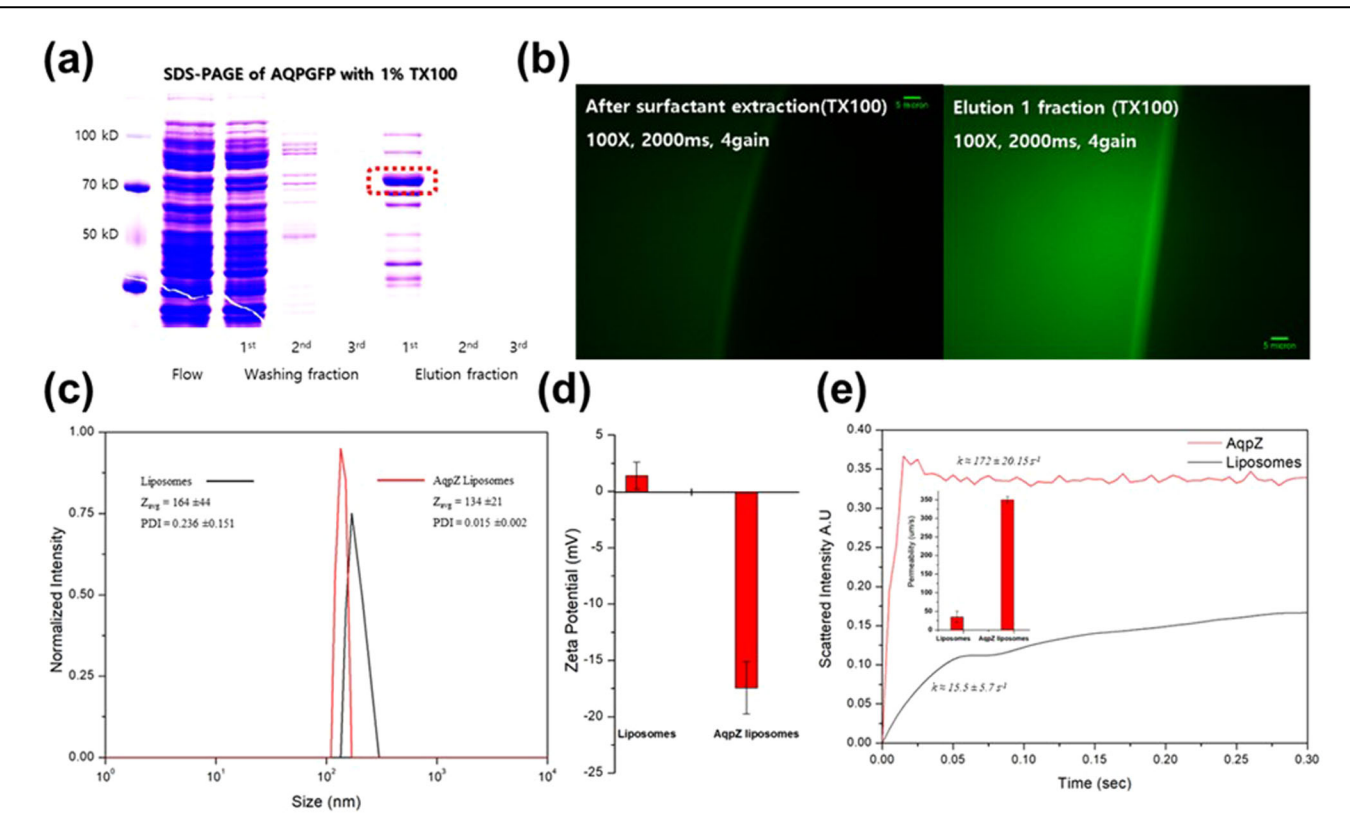


Fig. 3 | **Characterization of AqpZ protein. a** Gel electrophoresis (SDS-PAGE) of the purification fraction of GFP-fused AqpZ. The band in the red dash box displays purified GFP-fused AqpZ (size of ~70 kDa). **b** microscopic image of AqpZ expression. **c** DLS intensity graph of size analysis of liposomes and AqpZ liposomes. **d** Zeta potential of liposomes and AqpZ liposomes. **e** Stopped flow analysis of liposomes

and AqpZ liposomes with rate constants. The inset graph shows the calculated permeability of liposomes and AqpZ liposomes. The readings are based on at least three experiments. The scale bar in (b) is 5 μ m. The error bar represents the standard deviation (s.d.).

hyperosmolar sucrose solution using a stopped-flow mixing system. The osmotic gradient across the liposome-lipid bilayer leads to water efflux, which reduces the size of the liposomes and increases their light-scattering cross-section. The variation in scattered light intensity was analyzed using a fluorescence spectrometer (Fig. 3e). The liposomes show a low kinetic constant ($\approx\!15.5\pm5.7~s^{-1}$), while the AQP liposomes show a much higher rate constant ($\approx\!172\pm20.15~s^{-1}$) and reach a stable position in a short time interval of $<\!0.05~s$. Similarly, the liposome sample shows a lower net permeability (Pf = $35.12\pm11.36~\mu m~s^{-1}$) compared to the AQP liposome (Pf = $350.61\pm7.89~\mu m~s^{-1}$) calculated by Eq. (2). The increase in permeability of AQP-liposomes is due to the presence of AqpZ proteins, which provide an additional pathway for water molecules to move across the liposome bilayer in a short interval of time as compared to the slow diffusion of water molecules in the control liposome sample.

AQP AAO membrane fabrication

The coating processes prior to AQP immobilization on the AAO substrate are essential to fabricating a membrane with both high water permeability and salt rejection. Successful coating in each step was confirmed via XPS, AFM, and FESEM analyses of the membranes. A surface quantitative elemental analysis following each coating process (APTES, PDA, and AQP liposomes) was performed using XPS. Figure 4 shows the analysis results for substrates after each coating process. The silane functional group in APTES results in an increase in the concentration of silicon (Si) on the substrate surface after coating, which can be identified by analyzing the Si2p peak area (Fig. 4b; compare the uncoated substrate in Fig. 4a). The Si2p peak area decreases upon coating of PDA and AQP liposomes on the substrate (Fig. 4c and d). Moreover, the membrane without AQP liposomes has a low phosphorus (P2p) signal (Fig. 4e), whereas after AQP liposome coating, the concentration of phosphorus atoms (P2p) increases, indicating the

accumulation of lipid phosphate groups and confirming the presence of AQP liposomes on the substrate.

The bare substrate without any coating has uncovered pores, as shown in Fig. 5a. After silane functionalization and PDA coating, the pore size decreases, and a thin layer of PDA is clearly visible on the substrate (Fig. 5b). Liposome immobilization was performed by using previously reported electrokinetic phenomena 10, as this method ensures uniform coating of liposomes on the substrate pores without aggregation (Fig. 5c). After AQP liposome fixation, a protective layer was introduced by alternate coating of PDA and histidine in three cycles. The self-polymerizing molecule PDA binds with amine groups on the silane-functionalized AAO and the lipids. This coating layer protects the AQP liposomes and fills the voids if any between the AQP liposomes and substrate, to restrict the diffusion of solutes and minimize defects. Histidine can also bind dopamine and helps increase the salt rejection property because of its zwitterionic property.

The surface roughness was also analyzed using AFM after each step. The decrease in the surface roughness of the AQP membrane indicates the coating quality or uniform coating layer of proteoliposomes on the substrate surface, which ensures the functionality of the aquaporin protein after coating 10,31,32 . The formation of liposome/proteoliposome aggregates (which may affect the structure and performance of the aquaporin protein) on the surface during coating indicates the formation of valleys, which consequently increases the surface roughness and thus decreases the performance of the AQP membrane. Therefore, roughness is an important parameter to analyze the quality of the coating on the substrate. The bare AAO substrate has the highest surface roughness (Rq) of 19.6 ± 3.2 nm (Fig. 5d), while the surface roughness decreases to 12.4 ± 2.53 nm after surface functionalization with APTES and PDA in Fig. 5e, this decrease in roughness indicates

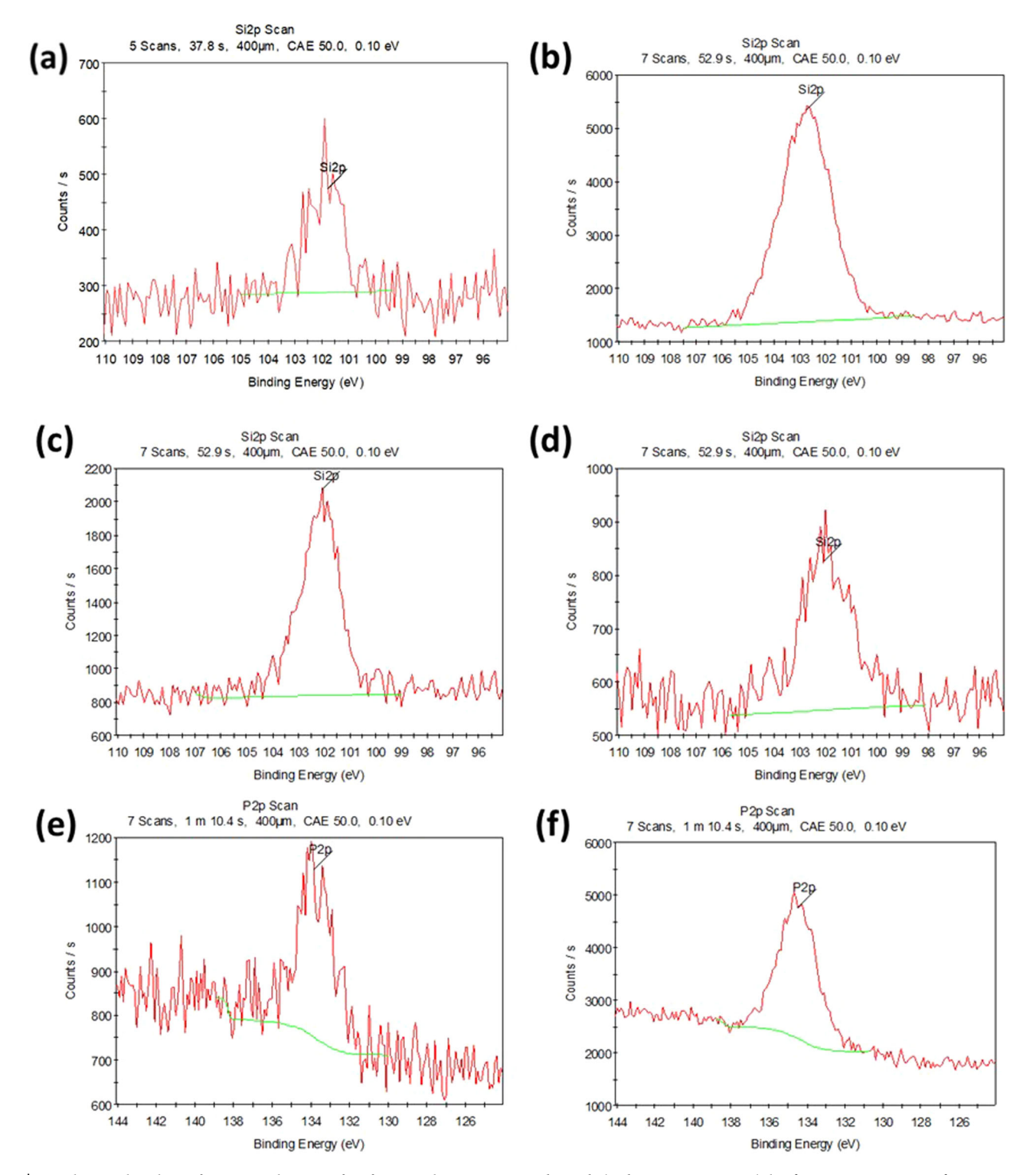


Fig. 4 | XPS elemental analysis of AAO membrane surface functionalization. a Control sample (without APTES coating). b After APTES coating. c After PDA coating. d After AQP liposome coating (e) and (f) before and after AQP liposome coating.

that the surface functionalization covers the valleys of the pristine substrate and forms a cushioning support layer for uniform AQP liposome coating on the substrate. The surface roughness further decreases to $9.16\pm1.09~\mathrm{nm}$ after AQP liposome coating, as shown in Fig. 5f. This further decrease in surface roughness shows that AQP liposomes have been uniformly coated on the substrate and smoothes the valley on the pristine AAO substrate. The AQP AAO membrane surface morphology after water purification was also analyzed using FESEM and, as shown in Supplementary Fig. 1, there are no notable changes.

Water purification ability

To evaluate the performance of AQP-coated membranes, a laboratory-built custom FO chamber was used with an eddy-promoting spacer. The addition of the spacer creates turbulence that facilitates mass transfer. The water permeability of the AQP AAO membrane was tested under the FO system using a 2000 ppm NaCl FS and a 1 M sucrose DS. Unlike the uncoated AAO substrate, which did not reject salt due to its large pore size and high porosity, the liposome-coated AAO membrane without AQP proteins showed a decrease in water flux to 8.2 ± 1.59 LMH (L m⁻² h⁻¹) and a reverse

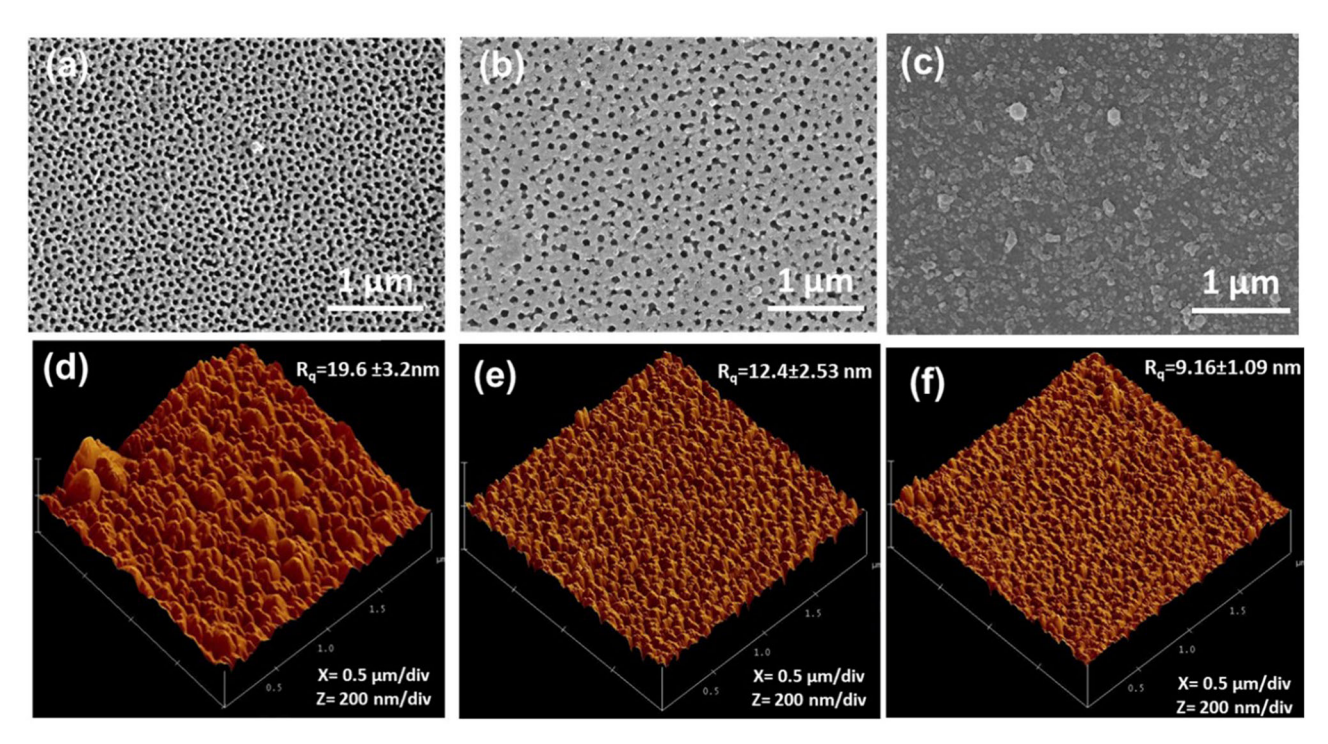


Fig. 5 | Surface morphological analysis of the membranes. a Before coating the membrane surface. **b** PDA functionalized substrate. **c** AQP membrane, after immobilization of AQP liposomes and subsequent PDA/His coating. **d** AFM surface

roughness analysis of the AAO membrane. **e** Surface roughness analysis after substrate functionalization. **f** AFM image after AQP liposome coating of the substrate.

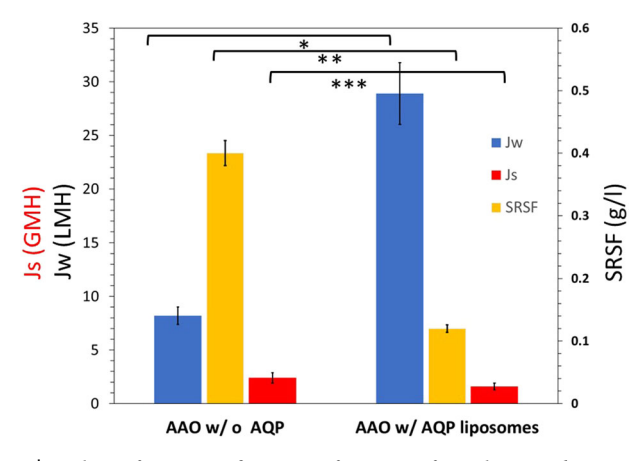


Fig. 6 | **Analysis of water purification performance of membranes.** The statistical analysis of the data was performed using Student's t-test (two-tailed) and the significant value was p < 0.05. The symbols *, **, *** show the p = 0.00013, p = 0.002 and p = 0.035, respectively. The error bar represents the standard deviation (s.d.).

solute flux of 2.4 ± 0.53 GMH (g m $^{-2}$ h $^{-1}$) in the FO test (Fig. 6). The low reverse solute flux was likely due to the complete coating of the liposomes on the AAO substrate surface, which has a low permeability to ions since the lipid bilayer membrane is intrinsically non-permeable to ions.

On the other hand, the AQP-containing AAO membrane showed high water permeability: the water flux was as high as 27.6 ± 3.6 LMH, with a reverse solute flux as low as 1.6 ± 0.26 GMH, demonstrating the activity of AQP in the liposomes. The AQP water channels provided additional pathways for water flow, increasing water flux while rejecting solute or salt compared to the liposome-coated membrane without AQP. To demonstrate the power of these aquaporin pathways to allow the transport of solute-free water, we also calculated the specific reverse solute flux (SRSF), a key parameter indicating the selectivity of the FO membrane. The SRSF is the ratio of the movement of solute particles to the movement of water. The

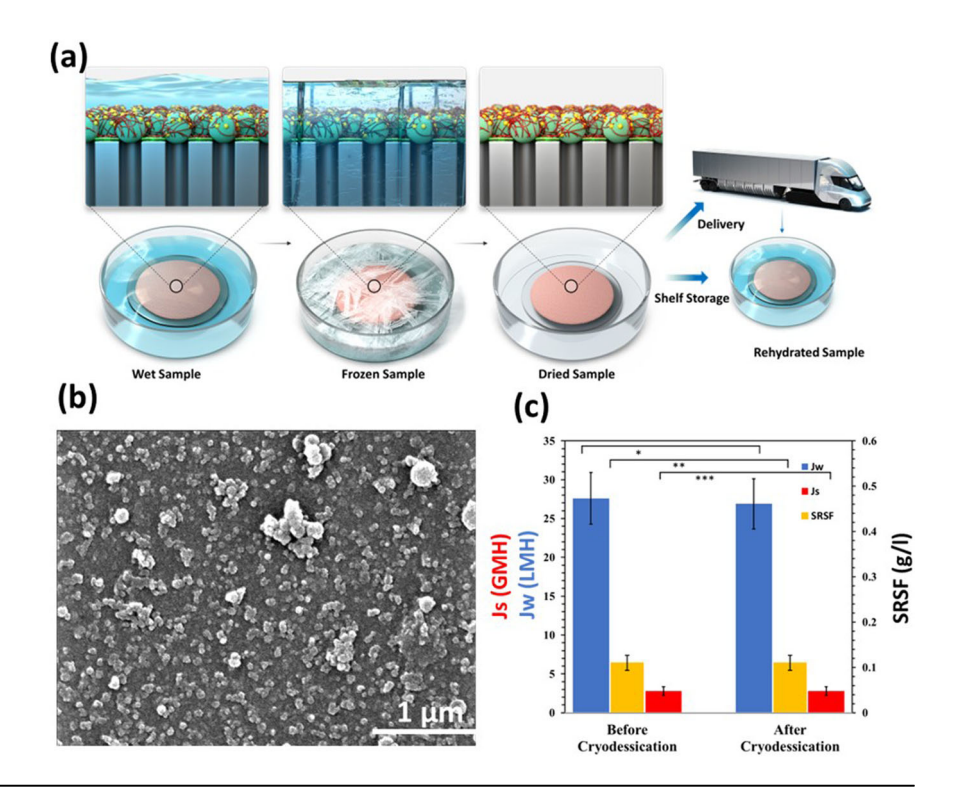
lower the SRSF value is, the higher the selectivity of the membrane. The AAO membrane with AQP shows a lower SRSF value (higher membrane selectivity) compared to the control AAO membrane (without AQP) mainly because of the increased water permeability and low solute diffusion due to the presence of highly surface-charged aquaporin proteins, which increase both the water permeability and the solute rejection. In addition, the ion rejection is mainly based on the lipid membrane (liposomes). This barrier is similar for membranes with and without AQP, but the water permeability increases significantly due to the presence of the aquaporin water channel, which in turn decreases the SRSF value. Furthermore, a high reverse solute flux value in the control membrane (liposomes) could indicate some defects in the membrane coating. Since the membrane coating was performed by electrokinetic interaction, where the modified particles move in the direction of the electric field, which is directly influenced by the charges of the particles (in this case liposomes)^{33–35}, the low charge of the liposomes may leave some defects, which in turn shows high salt movement across the membrane. Table 1 shows a comparison of the membrane reported here with previous literature reports^{36–40}. Our membrane shows superior water purification performance mainly due to the optimized fabrication of a substrate with low surface roughness and a channel-type porous structure, which supports the water permeability performance of AQP. As previously reported membranes mostly utilized polymeric substrates which have low porosity as well as non-channel-like pores which are unable to support the water permeability performance of pristine aquaporin liposomes as shown by several biophysical and stopped-flow analysis 10,21,41. Moreover, these membranes were fabricated mostly using interfacial polymerization (IP), in which the proteoliposomes were covered with a selective layer, most usually polyamide, so that most of the water permeability, as well as the salt rejection, was depended only on the characteristics of this selective layer or interfacial polymerization rather than on the proteoliposomes or AQPliposomes^{20,41,42}. Although we reported an electrokinetic coating method in our previous studies to uniformly coat a commercially available membrane for high water permeability, this membrane still does not fully support the permeability capabilities of aquaporin protein mainly due to the low porosity¹⁰. Finally, Doung et al. utilized the commercially available alumina

Table 1 | Comparison of different FO membranes

Membrane	Water flux (L m ⁻² h ⁻¹)	SRSF	Operating conditions	Ref.
Aquaporin inside a thin film composite membrane	8.8	0.45	DS: 1.5 M NaCl; FS: DIW	36
Graphene oxide aquaporin thin film nanocomposite (GO-AQP-TFC)	24.1	0.37	DS: 0.5 M NaCl; FS: DIW	37
Aquaporin A/S hollow fiber membrane (AQP-HF)	13.2	0.13	DS: 1 M NaCl; FS: DIW	38
Aquaporin biomimetic membrane	22.31	0.13	DS: 1 M NaCl; FS: DIW	39
TFC-layered silica-polysulfone (PSF)	31	0.24	DS: 1 M NaCl; FS: DIW	40
Silane-functionalized aquaporin-coated AAO membrane	27.6	0.11	DS: 1 M sucrose; FS: 2000 ppm NaCl	This study

Fig. 7 | Cryodesiccation process and analysis through FESEM and FO water purification.

a Schematic image of the cryodesiccation process and its possible importance in storability and transportability. **b** FESEM image of the membrane after 2 cycles of cryodesiccation (freeze-drying, rehydration, and then freeze-drying again before taking the FESEM image). **c** FO water purification analysis of the membrane. Statistical analysis was performed using Student's *t*-test (two-tailed) and the significant value was set at p < 0.05. where *, **, *** indicate non-significant values of 0.15, 0.225, and 0.135, respectively. The scale bar in (**b**) is 1 µm. The error bar represents the standard deviation (s.d.).



substrate to fabricate an aquaporin biomimetic membrane for water purification and it shows a salt rejection performance of only 45% due to the coating defects²⁴. It was observed that the defects in the reported study occur due to the non-optimization of the surface morphology of the substrate as well as the coating methodology. The uncontrolled chemical coating of aquaporin planar bilayer on the surface leads to defects or uncoated pores because the vesicle rupture leads to several shortcomings including irregular planar bilayer thickness, limited control over planar bilayer orientation as well as the uniformity or thickness control. Therefore, we overcome these problems by fabricating a substrate with a channel-like structure with controlled surface morphology as well as employing a uniform proteoliposome layer on the substrate surface, which offers high salt rejection with high water permeability capabilities.

Transportability and storability of the AQP-coated membranes

Previously reported AQP membranes have strict environmental requirements for storage, including a limited range of temperatures and humidity compatible with continuous hydration of the membrane before testing or after fabrication 41,43-45. These stringent requirements limit the transport, storage, and practicality of AQP membranes, thus precluding their industrial adoption and commercialization. A recently reported study shows that proteoliposomes, even in solution form at room temperature, lose their functionality within a week⁴¹, this is also in good agreement with the

previously reported studies mentioning the degradation or rupture of liposome structure in a dry environment. To verify this, we stored the membrane under ambient conditions (25 °C, 35% humidity) for 7 days without DI water, and analyzed the membrane surface morphology by FESEM analysis. The membrane shows the ruptured liposome structure (Supplementary Fig. 2), indicating that the dry environment makes the liposome structure brittle and prone to rupture, due to the evaporation of the suspension or water layer⁴⁶. To overcome these hurdles, we devised a cryodesiccation method in which AQP AAO membranes were freeze-dried for storage and then rehydrated immediately before use, as shown in Fig. 7a. Briefly, we froze the fabricated AQP AAO membranes at -80 °C and then sublimated the ice under low pressure in a vacuum chamber. After complete removal of the ice, we stored the sample under the same environmental conditions (25 °C and 35% humidity) for at least 7 days. The surface morphology of the rehydrated membrane was analyzed by performing FESEM analysis (Fig. 7b) and found that the liposomes remained intact on the substrate without any noticeable defects. Furthermore, to verify the activity of AqpZ activity after cryodesiccation water purification analysis was performed, the stored desiccated membrane was rehydrated with DIW at 4 °C for at least 1 h⁴⁷. After rehydration, water purification was carried out using the FO system described above. The rehydrated membrane showed minimal degradation of water purification performance in terms of water flux $(26.9 \pm 3.3 \text{ LMH})$ and reverse salt flux $(2.8 \pm 0.3 \text{ GMH})$, as shown in Fig. 7c,

which corresponds to ~98% of the performance shown by the AAO membrane before cryodesiccation. The statistical analysis shows no significant difference in the results of both membranes before and after cryodesiccation. This shows that the AQP liposomes remained intact following freeze-drying. In addition, we conducted a water purification experiment to evaluate the long-term stability of both AQP biomimetic membranes before and after cryodesiccation. The results, shown in Supplementary Fig. 3, demonstrated consistent water purification performance over 3 days of continuous operation. The observed decrease in water permeability after 12 h can be attributed to internal concentration polarization (ICP) within these membranes. This is primarily due to the dilution of the draw solution over time, which reduces the driving force and results in a decrease in water permeability. In short, the freeze-drying process preserves the AQP liposome structure as well as its function; thus, these membranes can be stored in a desiccated state semi-permanently and transported anywhere without specific environmental or storage conditions such as temperature and humidity. The extension of this work is being done to further enhance the mechanical strength of the substrate material. Additionally, the membrane's performance will be analyzed under harsh conditions, such as in hydraulic pressure-based water desalination (reverse osmosis), and its efficacy will be evaluated with various fluid types, including biological and agricultural wastewater.

In conclusion, we present a solution for two major problems associated with AQP biomimetic membranes: low water permeability, mainly due to the structure of the substrate, and transportability, which has previously required specific environmental conditions for AQP biomimetic membrane storage. To overcome these long-existing hurdles, we fabricated a highly porous ceramic-based AAO substrate and coated it with an AQP biomimetic membrane, which showed high water permeability (27.6 \pm 3.6 LMH or 1.6 ± 0.26 GMH) and a superior membrane selectivity of 0.11 g L⁻¹. This high-performance AQP vesicle-embedded membrane enables water purification with high throughput even at lower driving forces. Therefore, this technology could efficiently save energy during desalination and water reuse. Furthermore, to increase the longevity and transportability of AQPembedded membranes while preserving the membrane structure and functions, we implemented a cryodesiccation process. Cryodesiccated membranes can be stored in a desiccated state and transported without the need for specific environmental conditions in terms of humidity and temperature, widening the industrial adaptability of this emerging class of water purification materials.

Methods

Materials and chemicals

The chemicals, 10x phosphate-buffered saline (PBS, pH = 7.4), sucrose (C₁₂H₂₂O₁₁), sodium chloride (NaCl), ethylene glycol dimethacrylate (EGDMA), monobasic sodium phosphate (NaH₂PO₄),1-hydroxycyclohexyl phenyl ketone (Irgacure184), imidazole, dopamine hydrochloride, and lysozyme Triton X-100, were purchased from Sigma-Aldrich (USA). Polycarbonate track-etched (PCTE) substrates (Whatman Nuclepore) were purchased from Sterlitech Corporation (USA). Octyl β-Dglucopyranoside (ogp) was purchased from Carbosynth (UK), while the tris(hydroxymethyl) aminomethane (Tris) hydrochloride and Bio-Bead SM-2 absorbents were obtained from IBI Scientific (USA) and BIO-RAD (USA), respectively. The lipid compounds, 2-distearoyl-sn-glycero-3phosphoethanolamine-N-[amino(polyethylene glycol)-2000] (DSPE-PEG-NH₂), and 1,2-dioleoyl-sn-glycero-3-phosphocholine (DOPC) were purchased from Avanti Lipids. All chemicals were used in their original form unless otherwise noted.

AAO substrate fabrication

The support membrane was fabricated by the anodic aluminum oxidation (AAO) process (Fig. 1). First, a mechanically and electrochemically polished high-purity aluminum sheet (99.999%, 1 mm thickness) was prepared. The highly reflective aluminum sheet was exposed to anodization in an oxalic acid solution (0.3 M) at an

electrolyte temperature of 0 °C for 30 h with a bias current of 2 mA cm⁻². Which results in the formation of a nanoporous layer on the aluminum surface. The aluminum layer was removed through an etching process using a CuCl2-based aluminum etchant leaving behind a thin alumina sheet with nanopore openings on one side sealed by a barrier layer on the other side. To achieve channel-like alumina nanopores, the barrier layer that forms during the anodization process must be removed. The side of the substrate with nanopore openings was covered with polydimethylsiloxane (PDMS) and the sample was immersed in the alumina etchant. The etching process was performed for 8 h at 35 °C in a 0.1 M phosphoric acid solution, resulting in the formation of different pore sizes on the bottom and top sides. To synthesize the desired pore size in the AAO membrane, the etching process time was optimized, and it was observed that the duration of the etching process had a direct correlation with the widening of the pores, that is, a rate of 0.7 nm min⁻¹. This can be attributed to the fact that a longer etching time allows for more extensive oxide removal, resulting in a widening of the pore diameter.

Aquaporin Z (AqpZ) protein synthesis and analysis

Recombinant E. coli C41 strain containing the green fluorescent protein aquaporin-Z (GFP-AqpZ) expression vector was grown in Luria broth media at 37 °C overnight, followed by GFP-AqpZ vector induction by the addition of 1 mM isopropyl-β-D-thiogalactopyranoside (IPTG) and reincubated at 18 °C for 24 h. Cells were harvested by centrifugation at 4000 × g for 5 min and resuspended in lysis buffer (50 mM NaH₂PO₄, 200 mM NaCl, 5 mM imidazole, pH 8.0) and lysed by sonication. The solution was centrifuged at $10,000 \times g$ for 20 min to remove cell debris and the supernatant was collected. To extract GFP-AqpZ from the insoluble pallets, 1% Triton X-100 was added and applied to the Ni-NTA column, followed by washing and elution with buffer (50 mM NaH₂PO₄, 200 mM NaCl, 250 mM imidazole, 1% Triton X-100, pH 8.0). The GFP-AqpZ protein was examined by running the eluted fractions on an SDS PAGE gel analysis and the purified GFP-AqpZ was quantified by using the BCA assay kit. The stock solution of AqpZ was prepared by performing centrifugation (1 mg ml^{-1}) and stored at $-80 \,^{\circ}\text{C}$ for further use.

AQP liposomes preparation

AQP-loaded liposomes were prepared using previously reported methods^{10,48}. Briefly, 1,2-dioleoyl-sn-glycero-3-phosphocholine (DOPC), PEGylated amine terminated lipid (DSPE-PEG-NHa), EGDMA and Irgacure184 were mixed in a molar ratio of 20:1:40:20. A multilamellar liposome (MLV) suspension was prepared employing film rehydration method and was extruded through a PCTE membrane with a pore diameter of 200 nm at least 21 times. To fabricate AQP-liposomes with lipid to protein ratio (LPR 200:1), the AqpZ stock solution was added to the liposome solution during the film rehydration step and subjected to overnight rotation. Detergent was then removed using nonpolar adsorbent Bio-Beads (1 g in 5 ml of proteoliposome solution) in a stepwise manner (the beads were replaced after every 3 h) for at least 12 h^{48,49}. After detergent adsorption, AqpZ-containing liposomes were extruded through a PCTE membrane to ensure homogeneity followed by polymerization using a UV cross-linker (BLX-E254, 245 nm, 40 W Vilber Lourmat) for 40 min.

AQP liposomes characterization

The activity of AQP was confirmed through reaction kinetics analysis with a stopped-flow apparatus (MOS-200 & MOS-200M, SFM 2000, Biologics Science Instruments, France). Briefly, the liposome solutions (liposomes with AQP and without AQP) were mixed with a hypertonic solution (0.6 M sucrose), which resulted in water efflux from liposomes and hence a decrease in the liposome size. At a specific emission wavelength of 577 nm, an escalation in the intensity of light scattering was measured to determine the change in the size of the liposome. The scattering data were fitted to an exponential decay model Eq. (1) and the osmotic permeability of the liposomes was calculated using Eq. (2)⁵⁰. Liposome surface charge and size were

analyzed by dynamic light scattering (DLS) using a Zeta Nano ZS (Malvern Instruments).

$$Y = A \exp(-kt) \tag{1}$$

where Y is the intensity of the light scattering signal, A is a negative constant, t is the time of recording, and k is the initial rate constant (s^{-1}).

$$P_{\rm f} = \frac{r_{\rm o}k}{3V_{\rm w}} \times \frac{C_{\rm in} + C_{\rm out}}{2C_{\rm out}^2} \tag{2}$$

where r_0 , $V_{\rm w}$, $C_{\rm in}$, and $C_{\rm out}$ represent the initial liposome radius, partial molar volume of water, osmolar concentration inside and outside of the liposomes, respectively.

Fabrication of AQP-coated membranes

Functionalization of the AAO substrate was carried out using a previously published protocol⁵¹. Briefly, the oxidized AAO membrane surface (oxygen plasma generator, CUTO-100LF, Femto, Korea) was silanized using 1% (3-aminopropyl) triethoxysilane (APTES) in acetone for 30 min at room temperature, followed by baking at 80 °C overnight. Then, the silanized surface was further functionalized with a mussel-inspired polydopamine (PDA) coating as follows: the AAO substrate was immersed in a PDA solution (0.2 mg ml⁻¹ dopamine in 10 mM Tris–HCl buffer, pH = 8.5) for 3 h. This resulted in the spontaneous formation of a thin coating on the surface. To ensure a uniform coating, the solution was agitated continuously during substrate immersion. After coating, the functionalized membrane was washed with deionized water (DIW) to remove unbound PDA.

The protocol developed by Fuwad and coworkers was implemented for the electrokinetic AQP liposome coating 10 . The functionalized substrate was stacked between two electrodes in a microchannel device, and the liposome solution was introduced through a syringe into the microchannels. After filling the solution, a 1 V was applied across the substrate for 1 h. After liposome coating, the surface was sequentially subjected to PDA coating for at least 3 h incubation in 10 mM Tris–HCl buffer at pH 8.6 with a concentration of 0.2 mg mL $^{-1}$, followed by the histidine coating for 1 h in 1× PBS buffer at pH = 7.4 with a concentration of 0.2 mg mL $^{-1}$. These coatings not only protect the AQP liposomes but also help in the closure of any vacant spaces left during AQP liposome immobilization. Figure 1 presents a schematic diagram of the complete process of fabricating the AQP AAO membrane.

Freeze drying of membranes

The AQP-coated AAO membrane immersed in water was frozen in a deep freezer at $-80\,^{\circ}$ C. After complete freezing, the membrane was desiccated at a low temperature ($-20\,^{\circ}$ C) under vacuum for $8-12\,h$ until complete removal of ice by sublimation. The membrane was then stored for further analysis.

Surface characterization and morphological analysis

Elemental characterization of the membrane surface after each coating step was performed using X-ray photoelectron spectroscopy (XPS, Thermo Scientific). Surface morphology characterization was performed using field emission scanning electron microscopy (FESEM) (Hitech S-4200) and atomic force microscopy (AFM) (Multimode IVa).

FO membrane fabrication

An FO system was used to analyze the water purification performance of the AQP-coated AAO membrane. The membrane cell contains a 2 mm deep flow channel on each side of the AQP AAO membrane with cocurrent flow of the feed solution (FS) (NaCl 2000 ppm) and draw solution (DS) (1 M sucrose). The membrane was tested in the active layer feed side (AL-FS) orientation. The membrane performance in terms of the water permeability (Js, LMH) was calculated using Supplementary Eq. (1). The reverse solute flux (Jw, GMH) was calculated through Supplementary Eq. (2), whereas the

specific reverse solute flux (SRSF, g L⁻¹) was calculated by using Supplementary Eq. (3). Results represent the average of three trials.

Data availability

The datasets used and/or analyzed during the current study are available from the corresponding author on reasonable request.

Received: 1 September 2023; Accepted: 23 January 2024; Published online: 15 February 2024

References

- Murata, K. et al. Structural determinants of water permeation through aquaporin-1. Nature 407, 599–605 (2000).
- Borgnia, M. J., Kozono, D., Calamita, G., Maloney, P. C. & Agre, P. Functional reconstitution and characterization of AqpZ, the *E. coli* water channel protein. *J. Mol. Biol.* 291, 1169–1179 (1999).
- Calamita, G. The Escherichia coli aquaporin-Z water channel. Mol. Microbiol. 37, 254–262 (2000).
- Lim, Y., Goh, K. & Wang, R. The coming of age of water channels for separation membranes: from biological to biomimetic to synthetic. Chem. Soc. Rev. 51, 4537–4582 (2022).
- Shen, J., Liu, G., Han, Y. & Jin, W. Artificial channels for confined mass transport at the sub-nanometre scale. *Nat. Rev. Mater.* 6, 294–312 (2021).
- Li, X. et al. Preparation of high performance nanofiltration (NF) membranes incorporated with aquaporin Z. J. Membr. Sci. 450, 181–188 (2014).
- Wang, H. L. et al. Mechanically robust and highly permeable AquaporinZ biomimetic membranes. *J. Membr. Sci.* 434, 130–136 (2013).
- Wang, H. et al. Preparation and characterization of pore-suspending biomimetic membranes embedded with Aquaporin Z on carboxylated polyethylene glycol polymer cushion. Soft Matter 16, 7274–7280 (2011).
- Zhao, Y. et al. Synthesis of robust and high-performance aquaporinbased biomimetic membranes by interfacial polymerizationmembrane preparation and RO performance characterization. *J. Membr. Sci.* 423–424, 422–428 (2012).
- Fuwad, A. et al. An electrokinetic approach to fabricating aquaporin biomimetic membranes for water purification. *Desalination* 452, 9–16 (2019).
- Fuwad, A., Ryu, H., Malmstadt, N., Kim, S. M. & Jeon, T. J. Biomimetic membranes as potential tools for water purification: preceding and future avenues. *Desalination* 458, 97–115 (2019).
- Zhao, Y., Wang, Y. N., Lai, G. S., Torres, J. & Wang, R. Proteoliposome-incorporated seawater reverse osmosis polyamide membrane: is the aquaporin water channel effect in improving membrane performance overestimated? *Environ. Sci. Technol.* 56, 5179–5188 (2022).
- Beratto-Ramos, A., Dagnino-Leone, J., Martínez-Oyanedel, J., Aranda, M. & Bórquez, R. Fabrication and filtration performance of aquaporin biomimetic membranes for water treatment. Sep. Purif. Rev. 51, 340–357 (2022).
- Lim, Y. J., Goh, K., Kurihara, M. & Wang, R. Seawater desalination by reverse osmosis: current development and future challenges in membrane fabrication—a review. J. Membr. Sci. 629, 119292 (2021).
- Yu, Y., Seo, S., Kim, I. C. & Lee, S. Nanoporous polyethersulfone (PES) membrane with enhanced flux applied in forward osmosis process. *J. Membr. Sci.* 375, 63–68 (2011).
- Zhao, C. & Qiao, Y. Characterization of nanoporous structures: from three dimensions to two dimensions. *Nanoscale* 8, 17658–17664 (2016).
- 17. Lim, Y. J., Lee, J., Bae, T. H., Torres, J. & Wang, R. Feasibility and performance of a thin-film composite seawater reverse osmosis

- membrane fabricated on a highly porous microstructured support. *J. Membr. Sci.* **611**, 118407 (2020).
- Lalia, B. S., Kochkodan, V., Hashaikeh, R. & Hilal, N. A review on membrane fabrication: Structure, properties and performance relationship. *Desalination* 326, 77–95 (2013).
- Karim, S., Ensinger, W., Mujahid, S. A., Maaz, K. & Khan, E. U. Effect of etching conditions on pore shape in etched ion-track polycarbonate membranes. *Radiat. Meas.* 44, 779–782 (2009).
- Tang, C., Wang, Z., Petrinić, I., Fane, A. G. & Hélix-Nielsen, C. Biomimetic aquaporin membranes coming of age. *Desalination* 368, 89–105 (2015).
- Tang, C. Y., Zhao, Y., Wang, R., Hélix-Nielsen, C. & Fane, A. G. Desalination by biomimetic aquaporin membranes: review of status and prospects. *Desalination* 308, 34–40 (2013).
- Patel, Y., Janusas, G., Palevicius, A. & Vilkauskas, A. Development of nanoporous AAO membrane for nano filtration using the acoustophoresis method. Sensors (Switzerland) 20, 1–26 (2020).
- Petukhov, D. I., Buldakov, D. A., Tishkin, A. A., Lukashin, A. V. & Eliseev, A. A. Liquid permeation and chemical stability of anodic alumina membranes. *Beilstein J. Nanotechnol.* 8, 561–570 (2017).
- Duong, P. H. H. et al. Planar biomimetic aquaporin-incorporated triblock copolymer membranes on porous alumina supports for nanofiltration. *J. Membr. Sci.* 409–410, 34–43 (2012).
- Kirby, C. & Gregoriadis, G. Dehydration-rehydration vesicles: a simple method for high yield drug entrapment in liposomes. *Bio/Technology* 2, 979–984 (1984).
- Liu, S. & O'Brien, D. F. Stable polymeric nanoballoons: Lyophilization and rehydration of cross-linked liposomes. *J. Am. Chem. Soc.* 124, 6037–6042 (2002).
- Hussain, M. T. et al. Freeze-drying cycle optimization for the rapid preservation of protein-loaded liposomal formulations. *Int. J. Pharm.* 573, 118722 (2020).
- Masuda, H. & Fukuda, K. Ordered metal nanohole arrays made by a two-step replication of honeycomb structures of anodic alumina. Science (1979) 268, 1466–1468 (1995).
- Han, E. D., Kim, B. H. & Seo, Y. H. Experimental verification of Poiseuille flow in nanochannels. *Jpn. J. Appl. Phys.* 58, 065001 (2019).
- Tong, J., Briggs, M. M. & McIntosh, T. J. Water permeability of aquaporin-4 channel depends on bilayer composition, thickness, and elasticity. *Biophys. J.* 103, 1899–1908 (2012).
- Azarafza, A. et al. Aquaporin-based biomimetic membranes for low energy water desalination and separation applications. *Adv. Funct. Mater.* 33, 2213326 (2023).
- Beratto-Ramos, A. et al. Optimization of detergents in solubilization and reconstitution of Aquaporin Z: a structural approach. *Biochim. Biophys. Acta Biomembr.* 1865, 184101 (2023).
- Wu, D., Qin, J. & Lin, B. Electrophoretic separations on microfluidic chips. J. Chromatogr. A 1184, 542–559 (2008).
- Hossan, M. R., Dutta, D., Islam, N. & Dutta, P. Review: electric field driven pumping in microfluidic device. *Electrophoresis* 39, 702–731 (2018).
- Van Den Heuvel, M. G. L., De Graaff, M. P., Lemay, S. G. & Dekker, C. Electrophoresis of individual microtubules in microchannels. *Proc.* Natl Acad. Sci. USA 104, 7770–7775 (2007).
- Xia, L., Andersen, M. F., Hélix-Nielsen, C. & McCutcheon, J. R. Novel commercial aquaporin flat-sheet membrane for forward osmosis. *Ind. Eng. Chem. Res.* 56, 11919–11925 (2017).
- Akther, N. et al. Employing the synergistic effect between aquaporin nanostructures and graphene oxide for enhanced separation performance of thin-film nanocomposite forward osmosis membranes. *Desalination* 498, 114795 (2021).
- Ren, J. & McCutcheon, J. R. A new commercial biomimetic hollow fiber membrane for forward osmosis. *Desalination* 442, 44–50 (2018).

- Liang, Z. et al. Performance evaluation of interfacial polymerisationfabricated aquaporin-based biomimetic membranes in forward osmosis. RSC Adv. 9, 10715–10726 (2019).
- Liu, X. & Ng, H. Y. Fabrication of layered silica-polysulfone mixed matrix substrate membrane for enhancing performance of thin-film composite forward osmosis membrane. *J. Membr. Sci.* 481, 148–163 (2015).
- Sharma, L. et al. Aquaporin-based membranes made by interfacial polymerization in hollow fibers: visualization and role of aquaporin in water permeability. *J. Membr. Sci.* 654, 120551 (2022).
- Grzelakowski, M., Cherenet, M. F. & Shen, Y. xiao & Kumar, M. A framework for accurate evaluation of the promise of aquaporin based biomimetic membranes. *J. Membr. Sci.* 479, 223–231 (2015).
- Li, Y., Qi, S., Tian, M., Widjajanti, W. & Wang, R. Fabrication of aquaporin-based biomimetic membrane for seawater desalination. *Desalination* 467, 103–112 (2019).
- Wang, M. et al. Layer-by-layer assembly of aquaporin z-incorporated biomimetic membranes for water purification. *Environ. Sci. Technol.* 49, 3761–3768 (2015).
- 45. Zhao, Y. et al. Optimization of aquaporin loading for performance enhancement of aquaporin-based biomimetic thin-film composite membranes. *Membranes* **12**, 32 (2021).
- Sironi, B. et al. Structure of lipid multilayers via drop casting of aqueous liposome dispersions. Soft Matter 12, 3877–3887 (2016).
- Van Winden, E. C. A., Zhang, W. & Crommelin, D. J. A. Effect of freezing rate on the stability of liposomes during freeze-drying and rehydration. *Pharm. Res.* 14, 1151–1160 (1997).
- Sun, G., Chung, T. S., Jeyaseelan, K. & Armugam, A. Stabilization and immobilization of aquaporin reconstituted lipid vesicles for water purification. *Colloids Surf. B Biointerfaces* 102, 466–471 (2013).
- Wang, H. et al. Highly permeable and selective pore-spanning biomimetic membrane embedded with aquaporin Z. Small 8, 1185–1190 (2012).
- 50. Hannesschläger, C., Barta, T., Siligan, C. & Horner, A. Quantification of water flux in vesicular systems. *Sci. Rep.* **8**, 1–8 (2018).
- Jani, A. M. M., Kempson, I. M., Losic, D. & Voelcker, N. H. Dressing in layers: layering surface functionalities in nanoporous aluminum oxide membranes. *Angew. Chem.-Int. Ed.* 49, 7933–7937 (2010).

Acknowledgements

This work was supported by the National Research Foundation of Korea (NRF) grant funded by the Ministry of Science and Technology Information and Communication (MSIT) (Nos. NRF-2019R1A2C1084787, NRF-2021R1A2C2003571 and RS-2023-00207801) and Korean Environmental Industry & Technology Institute (KEITI), Ministry of Environment (no. 2022002980004). The funder played no role in the study design, data collection, analysis and interpretation of data, or the writing of this manuscript.

Author contributions

A.F.—conceptualization, experimentation, data curation, and visualization, writing, and revision of draft; H.R.—experimentation, data curation, writing the original manuscript, revision, and schematic figure preparation; E.D.H.—experimentation (AAO substrate synthesis, substrate characterization), draft writing; J.H.L.—experimentation (aquaporin synthesis, characterization); N.M.—conceptualization, supervision, writing, and revision of draft; Y.R.K.—supervision, funding acquisition, writing and revision of draft; Y.H.S.—supervision, writing, and revision of draft; S.M.K.—supervision, funding acquisition, project administration, manuscript writing, and revision; T.-J.J.—conceptualization, supervision, project administration, funding acquisition, manuscript writing, and revision.

Competing interests

The authors declare no competing interests.

Additional information

Supplementary information The online version contains supplementary material available at https://doi.org/10.1038/s41545-024-00301-0.

Correspondence and requests for materials should be addressed to Sun Min Kim or Tae-Joon Jeon.

Reprints and permissions information is available at http://www.nature.com/reprints

Publisher's note Springer Nature remains neutral with regard to jurisdictional claims in published maps and institutional affiliations.

Open Access This article is licensed under a Creative Commons Attribution 4.0 International License, which permits use, sharing, adaptation, distribution and reproduction in any medium or format, as long as you give appropriate credit to the original author(s) and the source, provide a link to the Creative Commons licence, and indicate if changes were made. The images or other third party material in this article are included in the article's Creative Commons licence, unless indicated otherwise in a credit line to the material. If material is not included in the article's Creative Commons licence and your intended use is not permitted by statutory regulation or exceeds the permitted use, you will need to obtain permission directly from the copyright holder. To view a copy of this licence, visit http://creativecommons.org/licenses/by/4.0/.

© The Author(s) 2024